Chapter 10

Nonlinear Optical Enhancement with Plasmonic Core-Shell Nanowires

Rachel Grange
Institute of Applied Physics, Abbe Center of Photonics
Friedrich Schiller University Jena
Max-Wien-Platz 1, 07743 Jena, Germany
rachel.grange@uni-jena.de

10.1 Introduction

Many innovations in medicine, optoelectronics, or computer sciences rely on the development of new materials. To overcome the limitations of the well-established fields of semiconductor (silicon) and dielectric (glass fiber) materials, metal plasmonics recently demonstrated high performances [1]. Indeed, since semiconductors are limited in speed due to electric interconnects and dielectrics are limited in size due to the diffraction limit, metallic nanostructures seems to be ideal to reach higher speed and keep the size small, even though they exhibit resistive losses due to the physical nature of metal [2]. Therefore, hybrid nanomaterials are anticipated to be part of new solutions for recently described paradigms in sciences, e.g. optical nanocircuits [2]. Adapted from Brongersma and Shalaev [1],

Active Plasmonic Nanomaterials
Edited by Luciano De Sio

ISBN 978-981-4613-00-2 (Hardcover), 978-981-4613-01-9 (eBook)
www.panstanford.com

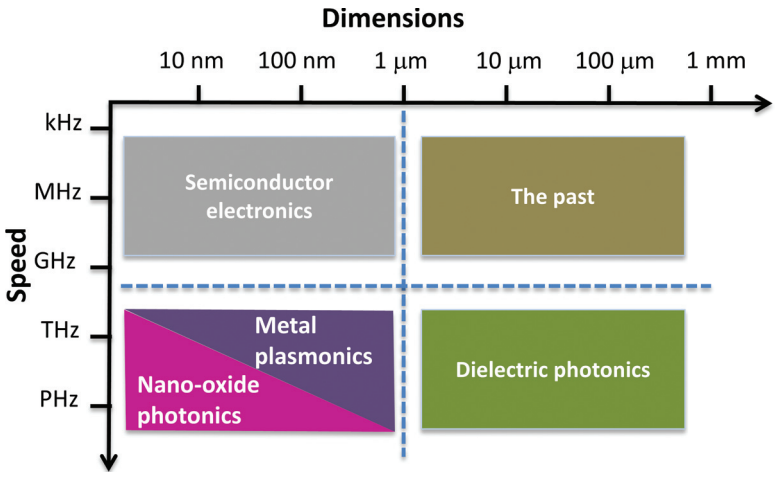

Figure 10.1 Widely studied materials, as semiconductor or dielectric, and their limitations in size and speed. Within the younger field of plasmonics emerges nano-oxide photonics based on hybrid nanostructures combining oxides and metallic nanomaterials. Adapted with permission from Ref. [1].

Fig. 10.1 summarizes the advantages and limitations of the above-mentioned materials.

Recently we showed that combining a metallic shell with a nano-oxide core, either a $BaTiO_3$ nanosphere [3], or a $KNbO_3$ nanowire [4], can increase the functionality of the materials. Well known in bulk form or thin films, oxides such as $LiNbO_3$ with a special crystal structure are ferroelectric, piezoelectric and possess a nonlinear optical polarizability suitable for daily applications in telecommunication [5]. Compared to semiconductors' planar structures suited for the infrared spectral range and semiconductor quantum dots that need to be as small as 2–10 nm to sustain optical resonances in the visible range for fluorescence microscopy [6], oxide nanoparticles, either spherical or anisotropic, cover more easily a broad spectral range taking advantage of nonlinear physical processes such as second-harmonic generation (SHG), mostly regardless of feature sizes. The multiplexing effect that seems to be lost in the nonresonant process such as SHG can be in fact facilitated by other mechanisms such as polarization dependency. Since SHG is a coherent process, the orientation of the particles may

be controlled and adjusted with polarization-sensitive illumination schemes [7]. The respective resonances can be engineered with metallic shells of different thicknesses taking advantage of plasmon-polaritonic effects. Moreover, oxide nanoparticles, particularly when thinly covered with a noble metal such as gold, seem to be much more biocompatible than metals used to fabricate quantum dots.

This chapter focuses on the nanowires hybrid nanostructures with an alkaline niobate core (Li-, K-, $NaNbO_3$) and a gold shell. Indeed, nanowires have interesting electronic and photonic properties suited for a wide range of applications such as nanolasers [8], solar absorbers [9, 10], generators [11], waveguides [12], or light-emitting diodes [13]. Biological applications are also of great interest and include nanowire-based devices such as nanoendoscopes or biosensors [14, 15]. We will present the state of the art of such hybrid nanostructures and their synthesis. Then we will show spectroscopic measurements and nonlinear optical experiments of single core-shell nanostructures to demonstrate the enhancement of the SHG using the localized surface plasmon resonance of the gold shell.

10.2 State of the Art

Bulk oxide materials such as lithium niobate ($LiNbO_3$), used in mobile telephones or optical modulators [5], still possess their optical properties at the nanoscale [16]. Furthermore, metals, first thought to be useless in optics except as mirrors, are now considered with great interest if the dimensions of their typical features are tens of nanometers, giving rise to resonant surface plasmon-polaritons in the optical spectral range [17]. Therefore, a large choice of materials for nanophotonics seems available besides well-known semiconductors. In this section, we give an overview of the fields of nonlinear photonics, nano-oxide wires or spheres, and core-shell plasmonic structures that are currently available.

The field of nonlinear photonics has been at the cutting edge of optics and quantum electronics research since the first experiment on SHG in 1961 [18]. Many important advances are reported since then as the demonstration of stimulated Raman scattering

[19], soliton generation in optical fibers [20], and Bose–Einstein condensation [21]. Combining those well-established concepts with the recent progress and freedom of designs in nanotechnology is paving the way for the investigations of many exciting and unprecedented nanoscale systems.

The study of semiconductor nanomaterials is a well-established field yielding useful application-oriented research with 2D quantum wells [22], 1D nanowires [23, 24], or 0D quantum dots [25]. Nano-oxide syntheses of anisotropic alkaline materials are reported since 2005 using various bottom-up methods such as template-assisted pyrolysis resulting in regular arrays of tubes [26], solution-phase synthesis resulting in rod-like structures [27], or hydrothermal synthesis producing free-standing nanowires with high aspect ratio [28]. Up to now, the crystal properties of nanomaterials have been well characterized using standard material science methods such as X-ray diffraction, scanning electron microscopy (SEM), or transmission electron microscopy. However, nonlinear optical or electro-optical properties have been rarely studied and almost no further processing steps such as doping or coating have been applied to those nanostructures. Only a few applications have already used these types of nanowires by combining the various physical properties of perovskite alkaline materials and the anisotropic shape at the nanoscale level. A nanometric SHG light probe manipulated by optical tweezers and capable of guiding light has been already described [29, 30]. In 2009, we demonstrated localized SHG light sources in optofluidic environments [31].

The first experiment with metallic nanoshells considered an Au_2S dielectric core surrounded by a gold shell without independent control of the core size [32]. Later on, Oldenburg et al. used dielectric cores, such as silica nanospheres, and varied the thickness of the shell or of the core to engineer optical resonances [33]. However, most of the core materials are found to possess no additional interesting properties and the nanoshells are used only to interact with the surrounding medium, for instance by local heating [34]. In 2010, we showed that a $BaTiO_3$ core with nonlinear optical properties can greatly benefit from the presence of a metallic nanoshell [3]. Basically, the strong localization of the light at the nanoscale associated with the excitation of localized

surface plasmon-polaritons at the metallic nanostructures entails the possibility to locally enhance the electric field by several orders of magnitude, boosting nonlinear responses, such as SHG. The demonstration of this strong resonance may also contribute to plasmonic laser research using a thin metal planar layer and semiconductor nanowires [35]. There have been some attempts to coat ZnO nanowires with gold; however, the coating was achieved only via sputtering [36, 37]. No chemical synthesis enabling to surround the complete surface of a nanowire has been reported or modelled.

10.3 Fabrication

In this section, we focus on bottom-up fabrication methods of alkaline nanowires, and especially $KNbO_3$. However, a top-down approach was also demonstrated for $LiNbO_3$ nanowires based on an ion-beam-enhanced etching method that reduces chemical stability of $LiNbO_3$ after ion-beam irradiation [38].

10.3.1 *Bottom-up Fabrication of the $KNbO_3$ Core*

Different chemistry-based approaches have been developed to fabricate crystalline alkaline niobate nanowires. Nanowires have been mainly produced by the sol-gel route [39], hydrothermal route [28, 40–44], and molten salt synthesis [45, 46].

For $KNbO_3$ nanowire used in the optical experiments of Sections 10.4 and 10.5, we used hydrothermal synthesis. This technique crystallizes substances under moderate temperatures (200–250°C) and high pressures. With an autoclave made of a thick-walled steel cylinder with a hermetic seal, anisotropic crystalline materials can be obtained in one step. Typical scanning electron microscopic images of bunch and isolated $KNbO_3$ nanowires can be seen in Fig. 10.2. This is a very convenient approach since a large amount of material can be fabricated in a one-step synthesis. Many synthesis parameters can be adjusted, such as temperature, time, pressure (by an external pressure or the degree of the autoclave filling), solid–liquid ratio, and additives, to control the properties of the end product. Thus, hydrothermal synthesis is powerful because

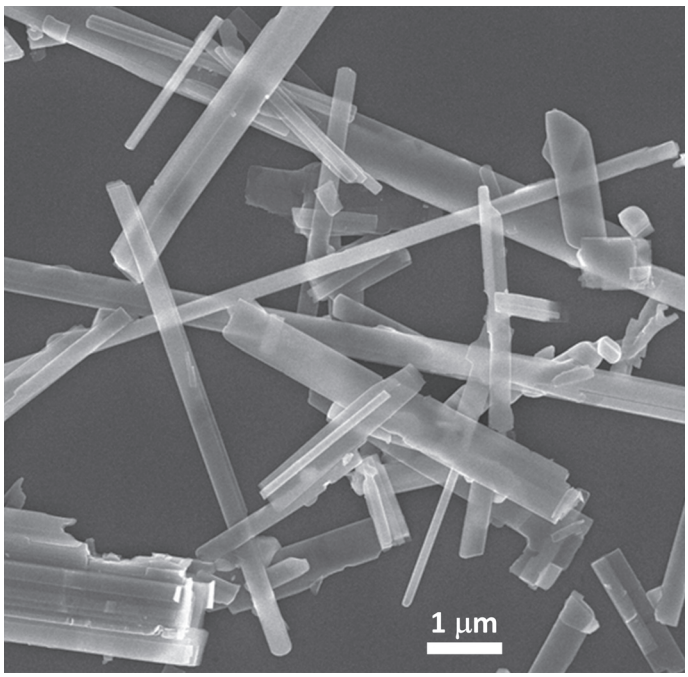

Figure 10.2 SEM images of typical $KNbO_3$ nanowires with aspect ratio up to 25.

many parameters can be modulated to control the particle size and morphology. Due to its simplicity, the hydrothermal technique has been widely studied and employed in inorganic synthesis for many years. A huge advantage of chemical synthesis in respect to chemical vapor deposition (CVD) or lithographic fabrication of nanowires is the ability to synthesize free-standing nanowires. Thus, no further step is needed to isolate or detach the nanowires, because no substrate is involved in the synthesis. If needed though, a substrate can be incorporated in the autoclave and nanoneedles have been demonstrated as well [47].

10.3.2 *Synthesis of the Gold Shell*

Since nonlinear optical processes such as SHG are generally inefficient at very small scale, we propose to take advantage of

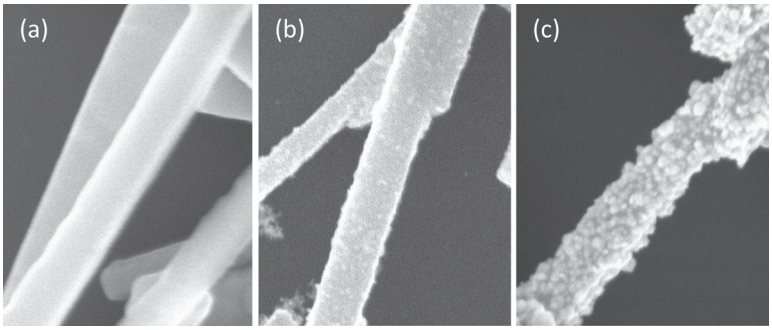

Figure 10.3 SEM image of $KNbO_3$ nanowires: (a) nanowires with polyelectrolyte coating, (b) nanowires seeded with gold nanoparticles, and (c) nanowire after the gold shell growth. The different nanowire diameter can be between 100 nm and 150 nm.

localized surface plasmon resonances from metallic nanostructures to strongly enhance nonlinear optical responses. We follow a typical silanization functionalization scheme [33] and demonstrate a $BaTiO_3$ core and gold shell structure [3]. Similarly, $KNbO_3$ nanowires are covered by a thin layer of gold to reach a near-infrared plasmonic resonance and enhance the SHG signal for optimized used as imaging probes or localized light source. The synthesis of the gold shell on a dielectric core is a process involving three stages: first, the functionalization of the core surface to make it positively charged (Fig. 10.3a); second, the adsorption of small gold particles negatively charged (seeds) onto the functionalized core (Fig. 10.3b); and third, the growth of the gold shell on the previous seeded structure (Fig. 10.3c). We follow Duff et al. for the synthesis of the gold seeds [48]. The seeds have a diameter of 1–5 nm, a negative surface charge, and a narrow size dispersion. Then the nanowire surface needs to be functionalized. Several schemes can be followed to make the nanowire positively charged, either amino silane layer as in [3] or by using a polymer (PDACMAC) to coat silica spheres [49]. Recently, we demonstrated the advantage of polymer concerning the functionalizing of $KNbO_3$ nanowires, since the seeding is much more uniform than with the amino silane process [4]. After the adsorption of the gold seeds, the nanowire is supposed to be uniformly covered

by them. The final step is the shell growth around the seeds using an appropriate reducing agent, here hydroxylamine.

The resulting core-shell nanowire is not smooth (see Fig. 10.3c), but if the gold islands are touching each other, the collective oscillation of electrons can take place and consequently become a localized surface plasmon resonance.

10.4 Single Nanowire Spectrosocopy Measurements

The plasmonic resonances of the gold-coated $KNbO_3$ nanowires are studied by performing single particle spectroscopic measurements. Since the nanostructures are non-spherical and with large size distributions due to the chemical synthesis processes, ensemble measurements in a colloidal suspension are not possible. As the core-shell nanowires are produced in liquid environment, we drop them on a glass slide with a pipette. The glass substrates are patterned with numbers to recognize the position of the nanoparticles, either under an optical microscope or by SEM. The spectroscopic setup consists of an inverted microscope with a pinhole in the image plane to select the collected area with a spatial resolution of 1.6 μm. This enables precise measurements with a limited background signal due to the selective pinhole. Extinction measurements are done in transmission with bright field illumination of the single gold-covered $KNbO_3$ nanowire. Figure 10.4 shows the extinction spectrum of a single core-shell nanostructure with length and diameter of approximately 1.5 μm and 80 nm, respectively. We measured resonant peaks slightly below 700 nm and around 900 nm. According to the simulations (see next section), there are several core radii and thicknesses of the gold shell that exhibit plasmonic resonances close to such resonances. The geometry of the current wire corresponds to a shell thickness of 7.5 nm for a core radius of 35 nm to match with the resonance at 900 nm and to a shell thickness of 15 nm for the resonance at 700 nm. Those two different thicknesses are probably due to the nonhomogeneous gold shell along the nanowires. In nonlinear optical measurements, we therefore expect an enhancement of the excitation wavelength slightly below 700 nm and a strong enhancement at around 900 nm.

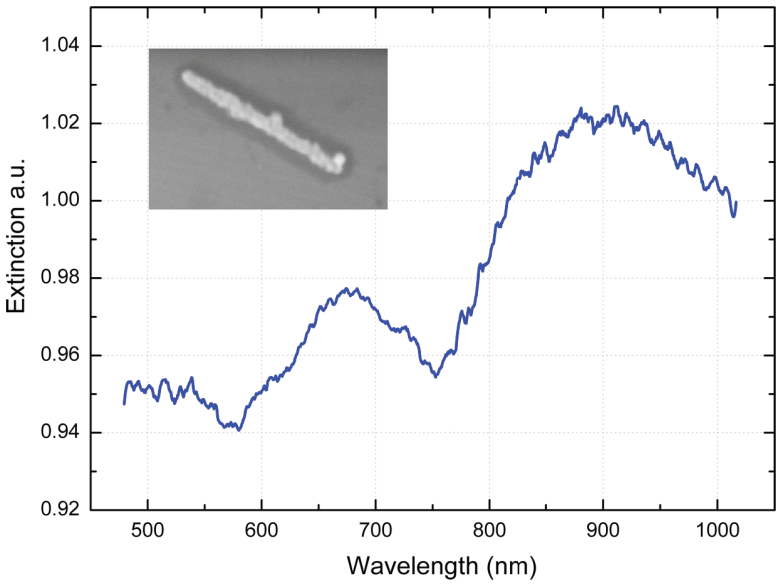

Figure 10.4 Single-wire spectroscopic measurements of the core-shell wire shown in the inset with length and diameter of approximately 1.5 μm and 80 nm, respectively. Adapted with permission from Ref. [4].

10.5 Nonlinear Optical Measurements

The alkaline nanowires, such as $KNbO_3$, with non-centrosymmetric crystal structures possess second-order optical properties. Such nonlinear effect scales with the square of the electric field, and since this is a volume effect with the sixth power of the nanoparticle radius [50], contrary to weak surface SHG effect of centrosymmetric materials [51, 52]. The optical response is expressed by the polarization P as a power series of the electric field E as

$$\vec{P} = \varepsilon_0 \chi_1 \vec{E} + \varepsilon_0 \chi_2 \vec{E}^2 + \varepsilon_0 \chi_3 \vec{E}^3 + \ldots \qquad (10.1)$$

where ε_0 is the permittivity of free space and χ_i is the ith-order nonlinear optical susceptibility tensor [53]. Each χ_i represents a different optical effect that can be summarized as follows for a physical understanding of Eq. 10.1. χ_1, the linear susceptibility, is related to absorption and reflection of light. χ_2 encompasses sum and difference frequency generation such as SHG. χ_3 describes

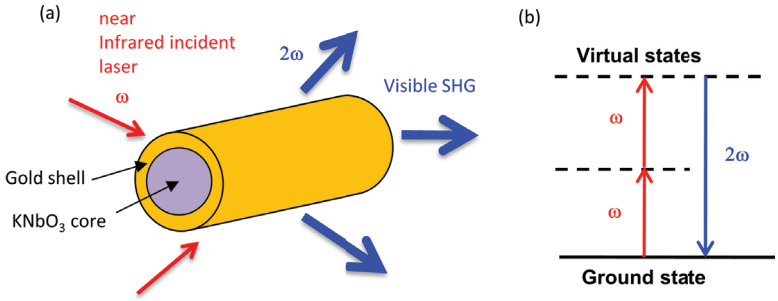

Figure 10.5 (a) Diagram of the SHG mechanism in a core-shell nanowire. The SHG arrows are bold to sketch the enhancement. (b) Energy diagram of the physical SHG mechanism.

multiphoton absorption, third harmonic generation, or coherent anti-Stokes Raman scattering.

To illustrate the SHG effect, Fig. 10.5a shows a core-shell nanowire optically excited at a fundamental frequency ϖ; it emits the optical signal at the exact doubled frequency 2ϖ. The corresponding energy diagram of the SHG mechanism is displayed in Fig. 10.5b, where two photons are simultaneously reaching a virtual energy state prior to be recombined in a single photon of half the wavelength or doubled frequency.

The setup for the nonlinear optical characterization of the SHG signal is shown in Fig. 10.6. A near-infrared laser light is slightly focused onto a sample by a $10\times$ objective, and the $100\times$ objective collects the signal imaged through a 4f configuration. Filters are used to cut the fundamental frequency and detect only a narrow band around the SHG frequency onto an electron multiplying charges coupled device.

The measurement of the SHG signal of single core-shell nanowires uses the home-built transmission microscope setup described in Fig. 10.6 and with more details in Ref. [54]. The laser can be tuned from 690 nm up to 1040 nm wavelength. The averaged laser power incident on the wires ranges between 50 mW and 70 mW with a spot size of 4 μm, therefore illuminating the whole wire uniformly. We used the spectroscopically characterized core-shell wire (Fig. 10.4) and a bare $KNbO_3$ nanowire, both lying on a

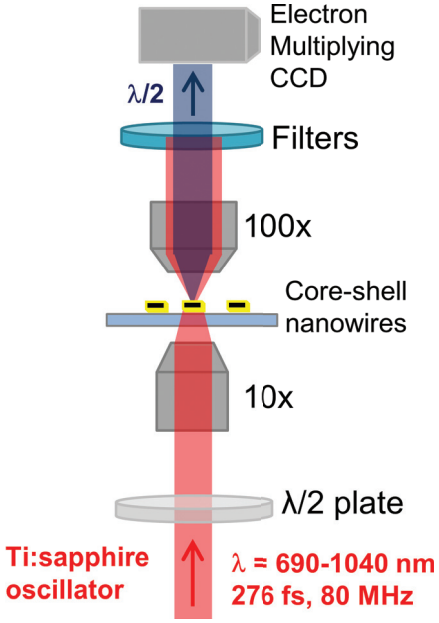

Figure 10.6 Setup for measuring SHG from individual nanowires dried on a microscope glass slide.

glass substrate. The length and diameter of the gold-coated wire are approximately 1.5 μm and 80 nm, respectively, and that of the bare wire are 2 μm and 150 nm, respectively.

In Fig. 10.7, the results of the SHG measurements from the bare and the core-shell wire are displayed. The SHG responses of both wires are plotted from the excitation wavelength of 700 nm up to 1040 nm. The bare wire exhibits a nearly constant SHG output over the measured spectral range. But the core-shell nanowire shows an enhanced output at larger wavelengths with a peak position identified at 900 nm.

We normalized the SHG output of both wires on the respective wire volume and the pulse peak power to be able to calculate the enhancement between the bare and core-shell wire. The enhancement factor is plotted along the measurement curve of Fig. 10.7 and shows its highest value at an excitation wavelength of 960 nm reaching an enhancement of 250 times. Below 700 nm, it is

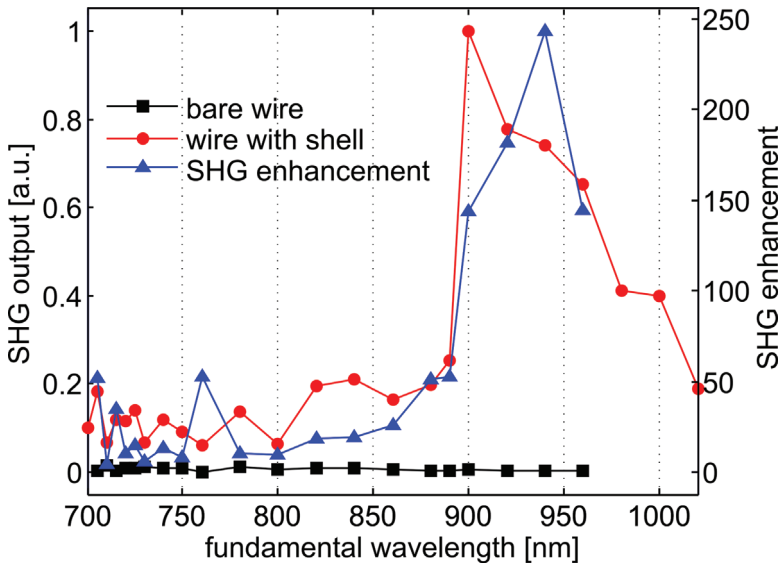

Figure 10.7 Measurement of SHG output and enhancement factor over excitation wavelength of a core-shell nanowire with a core radius of 35 nm and a shell thickness of 7.5 nm. Adapted with permission from Ref. [4].

not possible to reliably measure the SHG due to the laser wavelength limitation.

To compare this experimental result with the expected value from the theory, we model a typical core-shell structure. With these simulations, we can analyze the optical measurements and determine the best geometrical parameters of gold shell and core radius.

The optical response to the excitation at the fundamental frequency and the emission of the generated second harmonic are calculated analytically by the expansion of the electric and magnetic fields into cylindrical harmonics [55–57]. The SHG is treated in the undepleted pump approximation, i.e., the fundamental field in the core induces a nonlinear polarization at the second-harmonic frequency. The interaction between fundamental and second harmonic as well as the depletion of the fundamental wave are neglected. A more detailed description of the method can be found in Ref. [4]. The induced nonlinear polarization coefficients d_{ij}

within the core are given by [53, 58]

$$\begin{pmatrix} P_x^{\mathrm{NL}}(2\omega) \\ P_y^{\mathrm{NL}}(2\omega) \\ P_z^{\mathrm{NL}}(2\omega) \end{pmatrix} = 2\varepsilon_0 \begin{pmatrix} 0 & 0 & 0 & 0 & d_{31} & 0 \\ 0 & 0 & 0 & d_{32} & 0 & 0 \\ d_{31} & d_{32} & d_{33} & 0 & 0 & 0 \end{pmatrix} \begin{pmatrix} E_x(\omega)^2 \\ E_y(\omega)^2 \\ E_z(\omega)^2 \\ 2E_y(\omega)\,E_z(\omega) \\ 2E_x(\omega)\,E_z(\omega) \\ 2E_x(\omega)\,E_y(\omega) \end{pmatrix} \tag{10.2}$$

Because the electric field at the fundamental frequency ω has only an E_x and an E_y component, the induced nonlinear polarization is z-polarized and second-harmonic emission is, therefore, TE (transverse electric) polarized.

We calculated the SHG (in analogy with two photon excitation) cross section σ_{SHG} both for bare $KNbO_3$ nanowires and for nanowires with an additional gold shell. The cross section is given by

$$\sigma_{\mathrm{SHG}} = \frac{\hbar\omega}{2}\frac{P_{\mathrm{SHG}}}{I_{\mathrm{in}}^2} \tag{10.3}$$

where P_{SHG} is the emitted second-harmonic power per cylinder length, I_{in} is the incident intensity, and $\hbar\omega$ is the photon energy at

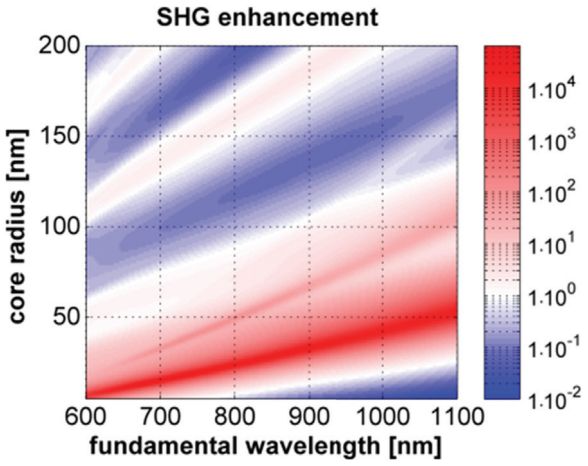

Figure 10.8 Simulation of the optical properties of $KNbO_3$ nanowires: resulting SHG emission enhancement. Adapted with permission from Ref. [4].

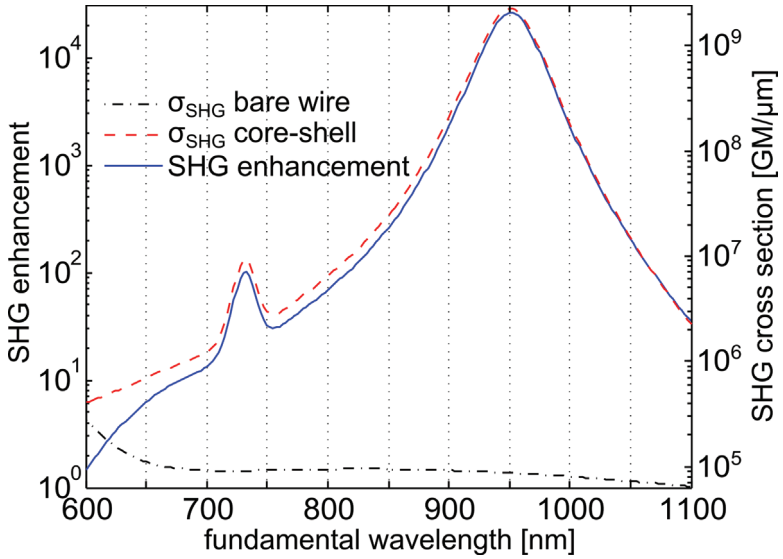

Figure 10.9 Simulated results for the SHG enhancement and SHG emission cross section of a core-shell nanowire with a core radius of 35 nm and a shell thickness of 7.5 nm. Adapted with permission from Ref. [4].

the fundamental frequency. The SHG enhancement due to the gold shell

$$\Gamma = \frac{\sigma_{\mathrm{SHG}}(\text{core-shell})}{\sigma_{\mathrm{SHG}}(\text{bare wire})} \tag{10.4}$$

is shown in Fig. 10.8. All resonances lead to an enhanced second-harmonic emission. However, the enhancement due to the lowest energetic fundamental resonance is by far the strongest and reaches values well above 10^4.

Figure 10.9 shows the SHG emission cross section of a core-shell and bare wire as well as the SHG enhancement versus the fundamental wavelength. In contrast to the simulation results introduced in Fig. 10.8 for all kinds of radius, here only the specific core radius of 35 nm for the $KNbO_3$ was taken into account. The simulated enhancement of the second harmonic has its peak at 950 nm and reaches a value of 30,000, which is about two orders of magnitude larger than the measured value of 250. This discrepancy can be due to several factors. In the simulation, we assume a

perfectly smooth gold shell and a plane wave excitation. But both conditions are not fully realized in the experiment. Indeed the shell is quite rough, and the nanowire is not perfectly cylindrical.

10.6 Conclusion

In this chapter, we showed how to enhance nonlinear optical signals as SHG with the growth of a plasmonic gold shell around $KNbO_3$ nanowires. We tested two types of functionalization to obtain the smoothest gold nanoshell. The gold shell with polyelectrolyte shows a more uniform coverage than silanized wires. We performed spectroscopic and SHG measurements on individual core-shell wires functionalized by the polyelectrolyte. Both measurements show a strong response slightly above 900 nm with an enhancement factor of the SHG signal of approximately 250 as compared to a bare wire. Such a strong signal enhancement is promising for applying the core-shell nanowire as a bright local light source in life sciences using the spectral filtering from nonlinear optical effects. Moreover, the chemically based synthesis is very simple to implement without any nanolithography processes involved.

Acknowledgments

The author thanks the Carl Zeiss Foundation, the DFG excellence program JSMC, and the Pro Chance Program of the Friedrich Schiller University for financial support. She is also grateful to Jessica Richter, Andrea Steinbrück, Anton Sergeyev, and Matthias Zilk for their support.

References

1. Brongersma ML and Shalaev VM (2010) The case for plasmonics. *Science* **328**, 440–441.
2. Engheta N (2007) Circuits with light at nanoscales: Optical nanocircuits inspired by metamaterials. *Science* **317**, 1698–1702.

3. Pu Y, Grange R, Hsieh C-L, and Psaltis D (2010) Nonlinear optical properties of core-shell nanocavities for enhanced second-harmonic generation. *Phys. Rev. Lett.* **104**, 207401–207405.
4. Richter J, Steinbrück A, Zilk M, Sergeyev A, Pertsch T, Tünnermann A, and Grange R (2014) Core-shell potassium niobate nanowires for enhanced nonlinear optical effects. *Nanoscale* **6**, 5200–5207
5. Wooten EL, Kissa KM, Yi-yan A, Murphy EJ, Member S, Lafaw DA, Hallemeier PF, Maack D, Attanasio DV, Fritz DJ, Mcbrien GJ, and Bossi DE (2000) A review of lithium niobate modulators for fiber-optic communications systems. *IEEE Sel. Top. Quantum Electron.* **6**, 69–82.
6. Michalet X, Pinaud FF, Bentolila LA, Tsay JM, Doose S, Li JJ, Sundaresan G, Wu AM, Gambhir SS, and Weiss S (2005) Quantum dots for live cells, in vivo imaging, and diagnostics. *Science* **307**, 538–544.
7. Hsieh C, Pu Y, Grange R, and Psaltis D (2010) Second-harmonic generation from nanocrystals under linearly and circularly polarized excitations. *Opt. Express*. **18**, 11917–11932.
8. Duan X, Huang Y, Agarwal R, Lieber CCM, and Fast CG (2003) Single-nanowire electrically driven lasers. *Nature* **421**, 241–245.
9. Colombo C, Heiß M, Grätzel M, and Fontcuberta i Morral A (2009) Gallium arsenide p-i-n radial structures for photovoltaic applications. *Appl. Phys. Lett.* **94**, 173108.
10. Cao L, Fan P, Vasudev AP, White JS, Yu Z, Cai W, Schuller J, Fan S, and Brongersma ML (2010) Semiconductor nanowire optical antenna solar absorbers. *Nano Lett.* **10**, 439–445.
11. Wang ZL and Song J (2012) Piezoelectric nanogenerators based on zinc oxide nanowire arrays. *Science* **312**, 242–246.
12. Voss T, Svacha GT, Mazur E, Mu S, Konjhodzic D, Marlow F, Müller S, and Ronning C (2007) High-order waveguide modes in ZnO nanowires. *Nano Lett.* **7**, 3675–3680.
13. Bao J, Zimmler MA, and Capasso F (2006) Broadband ZnO single-nanowire light-emitting diode. *Nano Lett.* **6**, 1719–1722.
14. Singhal R, Orynbayeva Z, Venkat R, Sundaram K, Niu JJ, Bhattacharyya S, Vitol EA, Schrlau MG, Papazoglou ES, Friedman G, and Gogotsi Y (2010) Multifunctional carbon-nanotube cellular endoscopes. *Nat. Nanotechnol.* **6**, 57–64.
15. Yan R, Park J, Choi Y, Heo C, Yang S, and Lee LP (2012) Nanowire-based single-cell endoscopy. *Nat. Nanotechnol.* **7**, 191–196.

16. Grange R, Dutto F, and Radenovic A (2011) Niobates nanowires: Synthesis, characterization and applications title, in *Nanowires/Book 2* (Hashim A, ed), Intech, pp. 509–524.
17. Atwater HA and Polman A (2010) Plasmonics for improved photovoltaic devices. *Nat. Mater.* **9**, 865.
18. Franken P, Hill A, Peters C, and Weinreich G (1961) Generation of optical harmonics. *Phys. Rev. Lett.* **7**, 118–119.
19. Eckhardt G, Hellwarth R, McClung F, Schwarz S, Weiner D, and Woodbury E (1962) Stimulated Raman scattering from organic liquids. *Phys. Rev. Lett.* **9**, 455–457.
20. Mollenauer LF, Stolen RH, and Gordon RH (1980) Experimental observation of picosecond pulse narrowing and solitons in optical fibers. *Phys. Rev. Lett.* **45**, 1095–1098.
21. Cornell E and Wieman C (2002) Nobel lecture: Bose–Einstein condensation in a dilute gas, the first 70 years and some recent experiments. *Rev. Mod. Phys.* **74**, 875.
22. Zory PS (1993) *Quantum Well Lasers*, Academic Press, San Diego.
23. Yazawa M, Koguchi M, Muto A, Ozawa M, and Hiruma K (1992) Effect of one monolayer of surface gold atoms on the epitaxial growth of InAs nanowhiskers. *Appl. Phys. Lett.* **61**, 2051–2053.
24. Yan RX, Gargas D, and Yang PD (2009) Nanowire photonics. *Nat. Photonics* **3**, 569–576.
25. Reed M, Randall J, Aggarwal R, Matyi R, Moore T, and Wetsel A (1988) Observation of discrete electronic states in a zero-dimensional semiconductor nanostructure. *Phys. Rev. Lett.* **60**, 535–537.
26. Zhao LL, Steinhart M, Yosef M, Lee SK, and Schlecht S (2005) Large-scale template-assisted growth of $LiNbO_3$ one-dimensional nanostructures for nano-sensors. *Sensors Actuators B* **109**, 86–90.
27. Wood BD, Mocanu V, and Gates BD (2008) Solution-phase synthesis of crystalline lithium niobate nanostructures. *Adv. Mater.* **20**, 4552–4556.
28. Magrez A, Vasco E, Seo JW, Dieker C, Setter N, and Forro L (2006) Growth of single-crystalline $KNbO_3$ nanostructures. *J. Phys. Chem. B* **110**, 58–61.
29. Nakayama Y, Pauzauskie PJ, Radenovic A, Onorato RM, Saykally RJ, Liphardt J, and Yang PD (2007) Tunable nanowire nonlinear optical probe. *Nature* **447**, 1098–1101.
30. Dutto F, Raillon C, Schenk K, and Radenovic A (2011) Nonlinear optical response in single alkaline niobate nanowires. *Nano Lett.* **11**, 2517–2521.

31. Grange R, Choi JW, Hsieh CL, Pu Y, Magrez A, Smajda R, Forró L, and Psaltis D (2009) Lithium niobate nanowires synthesis, optical properties, and manipulation. *Appl. Phys. Lett.* **95**, 143105–143105.
32. Zhou H, Honma I, Komiyama H, and Haus J (1994) Controlled synthesis and quantum-size effect in gold-coated nanoparticles. *Phys. Rev. B* **50**, 12052.
33. Oldenburg SJ, Averitt RD, Westcott SL, and Halas NJ (1998) Nanoengineering of optical resonances. *Chem. Phys. Lett.* **288**, 243–247.
34. Gobin M, Lee MH, Halas NJ, James WD, Drezek RA, West JL, and Gobin AM (2007) Near-infrared resonant nanoshells for combined optical imaging and photothermal cancer therapy. *Nano Lett.* **7**, 1929–1934.
35. Oulton RFRF, Sorger VJVJ, Zentgraf T, Ma RMR-M, Gladden C, Dai L, Bartal G, and Zhang X (2009) Plasmon lasers at deep subwavelength scale. *Nature* **461**, 629–632.
36. Prokes SM, Glembocki OJ, Rendell RW, and Ancona MG (2007) Enhanced plasmon coupling in crossed dielectric/metal nanowire composite geometries and applications to surface-enhanced Raman spectroscopy. *Appl. Phys. Lett.* **90**, 093105–093105.
37. Sinha G, Depero LEL, and Alessandri I (2011) Recyclable SERS substrates based on Au-coated ZnO nanorods. *ACS Appl. Mater. Interfaces* **3**, 2557–2563.
38. Sergeyev A, Geiss R, Solntsev AS, Steinbrück A, Schrempel F, Kley E-B, Pertsch T, and Grange R (2013) Second-harmonic generation in lithium niobate nanowires for local fluorescence excitation. *Opt. Express* **21**, 19012–19021.
39. Pribosic I, Makovec D, and Drofenik M (2005) Formation of nanoneedles and nanoplatelets of KNbO3 perovskite during templated crystallization of the precursor gel. *Chem. Mater.* **17**, 2953–2958.
40. An CH, Tang KB, Wang CR, Shen GZ, Jin Y, and Qian YT (2002) Characterization of $LiNbO_3$ nanocrystals prepared via a convenient hydrothermal route. *Mater. Res. Bull.* **37**, 1791–1796.
41. Shi H, Li X, Wang D, Yuan Y, Zou Z, and Ye J (2009) $NaNbO_3$ nanostructures: Facile synthesis, characterization, and their photocatalytic properties. *Catal. Letters* **132**, 205–212.
42. Wang GZ, Selbach SM, Yu YD, Zhang XT, Grande T, and Einarsrud MA (2009) Hydrothermal synthesis and characterization of $KNbO_3$ nanorods. *CrystEngComm* **11**, 1958–1963.

43. Wang GZ, Yu YD, Grande T, and Einarsrud MA (2009) Synthesis of $KNbO_3$ nanorods by hydrothermal method. *J. Nanosci. Nanotechnol.* **9**, 1465–1469.
44. Wu SY, Liu XQ, and Chen XM (2010) Hydrothermal synthesis of $NaNbO_3$ with low NaOH concentration. *Ceram. Int.* **36**, 871–877.
45. Santulli AC, Zhou H, Berweger S, Raschke MB, Sutter E, and Wong SS (2010) Synthesis of single-crystalline one-dimensional $LiNbO_3$ nanowires. *CrystEngComm* **12**, 2675–2678.
46. Li L, Deng J, Chen J, Sun X, Yu R, Liu G, and Xing X (2009) Wire structure and morphology transformation of niobium oxide and niobates by molten salt synthesis. *Chem. Mater.* **21**, 1207–1213.
47. Wang Y, Chen Z, Ye Z, and Huang JY (2012) Synthesis and second-harmonic generation response of $KNbO_3$ nanoneedles. *J. Cryst. Growth* **341**, 42–45.
48. Duff DG, Baiker A, and Edwards PP (1993) A new hydrosol of gold clusters. 1. Formation and particle size variation. *Langmuir* **9**, 2301–2309.
49. Caruso F and Möhwald H (1999) Preparation and characterization of ordered nanoparticle and polymer composite multilayers on colloids. *Langmuir* **15**, 8276–8281.
50. Kim E, Steinbrück A, Buscaglia MT, Buscaglia V, Pertsch T, and Grange R (2013) Second-harmonic generation of single $BaTiO_3$ nanoparticles down to 22 nm diameter. *ACS Nano* **7**, 5343–5349.
51. Dadap JI, Shan J, Eisenthal KB, and Heinz TF (1999) Second-harmonic Rayleigh scattering from a sphere of centrosymmetric material. *Phys. Rev. Lett.* **83**, 4045–4048.
52. Dadap JI (2008) Optical second-harmonic scattering from cylindrical particles. *Phys. Rev. B* **78**, 205322.
53. Boyd RW (2003) *Nonlinear Optics*, 2nd edn, Academic Press, Amsterdam.
54. Grange R, Brönstrup G, Kiometzis M, Sergeyev A, Richter J, Leiterer C, Fritzsche W, Gutsche C, Lysov A, Prost W, Tegude F-J, Pertsch T, Tünnermann A, and Christiansen S (2012) Far-field imaging for direct visualization of light interferences in GaAs nanowires. *Nano Lett.* **12**, 5412–5417.
55. Bohren CF and Huffman DR (2004) *Absorption and Scattering of Light by Small Particles*, Wiley-VCH, Weinheim.

56. Lee S-C (1992) Scattering by closely-spaced radially-stratified parallel cylinders. *J. Quant. Spectrosc. Radiat. Transf.* **48**, 119–130.
57. Wu D, Liu X, and Li B (2011) Localized surface plasmon resonance properties of two-layered gold nanowire: Effects of geometry, incidence angle, and polarization. *J. Appl. Phys.* **109**, 083540.
58. Dmitriev VG, Gurzadyan GG, and Nikogosyan DN (1999) *Handbook of Nonlinear Optical Crystals*, 3rd edn, Springer, Berlin.